

Fatigue Life Prediction of Fabric Braided Rubber Hose in Complicated Cyclic Motion

*Jin-Rae Cho¹⁾ and Young-Hyun Kim²⁾

¹⁾ *Department of Naval Architecture and Ocean Engineering, Hongik University, Sejong 339-701, Korea*

²⁾ *School of Mechanical Engineering, Pusan National University, Busan 609-735, Korea*

¹⁾ jrcho@hongik.ac.kr

ABSTRACT

This paper is concerned with the large deformation and the fatigue life of fabric braided rubber hose in complicated cyclic motion. The fabric braided hose exhibits the complex large deformation while moving along the specific cyclic path so that the fatigue damage is to be accumulated with the number of moving cycles. In order to assess the fatigue life according to the cyclic deformation and the initial mean strain, the modified fatigue model is employed. Two fatigue parameters were determined from the E-N curves that were obtained by the fatigue test using rubber specimens. The fatigue lives are calculated by making use of the rainflow cycle counting method and the Minor cumulative damage law. The numerical experiments are carried out to illustrate the fatigue prediction method, and the large deformation and fatigue life characteristics are parametrically investigated.

1. INTRODUCTION

Braking hose in the automotive hydraulic braking system plays an important role of delivering the driver's braking force to the brake disc cylinders via internal working oil. Since the traffic accidents caused by the oil leakage may lead to the fatal casualties, the braking hose should be elaborately designed to prevent the microcracking (Kwack and Choi, 2009), a main source of oil leakage, during the operation within the whole period of its warranty. The microcracking is mostly attributed to the complicated and large cyclic deformation of hose and to the interference with other adjacent vehicle components. For this reason, the braking hose is in the lamination composition of pure rubber layers and fabric braided layers to effectively prevent the oil leakage and to suppress the excessive large deformation (Entwistle, 1981; Cho et al., 2013). The fabric braided layers are composed of periodic warp and fill tows in the complex pattern, so those exhibit the anisotropic behavior even though their base materials are isotropic material (Cho et al., 2006; Xu et al., 2012; Chuda-Kowalska and Garstecki, 2016). Because of the anisotropic behavior of fabric braided layers, the whole braking hose

exhibits the inherent out-of-plane deformation during the steering and bump/rebound motions of vehicle (Cho et al., 2013). And, it becomes one of crucial factors in the design of oil leakage-proof high-durable braking hose, which produces the interference-free deformed configuration, by utilizing the computer-aided simulation.

The hose cyclic path is not unique but manifold depending on the combination of the steering and bump/rebound motions of vehicle (Cho et al., 2015). So, a number of major cyclic paths that characterize the hose deformed layout should be identified and numerically interpolated for the numerical simulation. For this reason, the hose deformed configuration for the specific hose cyclic path and the resulting fatigue life have been traditionally evaluated by experiments. However, this approach is highly cost- and time-consuming, and furthermore it leads to the hose layout design of trial and error. To overcome the demerits of experimental approach, the attempts to apply the analytical and computational methods have been attempted by several investigators.

As an extension of our previous work (Cho et al., 2013; 2015) on the braking hose, this paper intends to investigate the characteristics of hose large deformation and fatigue life to the hose cyclic path. Four representative cyclic paths are chosen, and the large deformation and fatigue analyses are carried out for each cyclic path. The homogenization, path interpolation and fatigue evaluation methods are integrated, and the variation of the maximum in-plane and out-of-plane deformations and the critical fatigue life cycles are comparatively investigated to the hose cyclic path.

2. LARGE DEFORMATION OF

Fig. 1(a) represents a typical braking hose assembled in the front braking system, where one end is fixed to the main body of vehicle while the other end, called the movable end throughout this manuscript, is attached to the tire assembly using a strut. Hence, the hose movable end is to be moved along with the tire motion, and hence the entire braking hose is forced to be deformed. The vehicle motion could be classified into the horizontal steering mode and the vertical bump/rebound mode. Here, the bump/rebound motion is resulted from the relative vertical movement of tire with respect to the vehicle at quick stop or start, or when the vehicle is running over cleats.

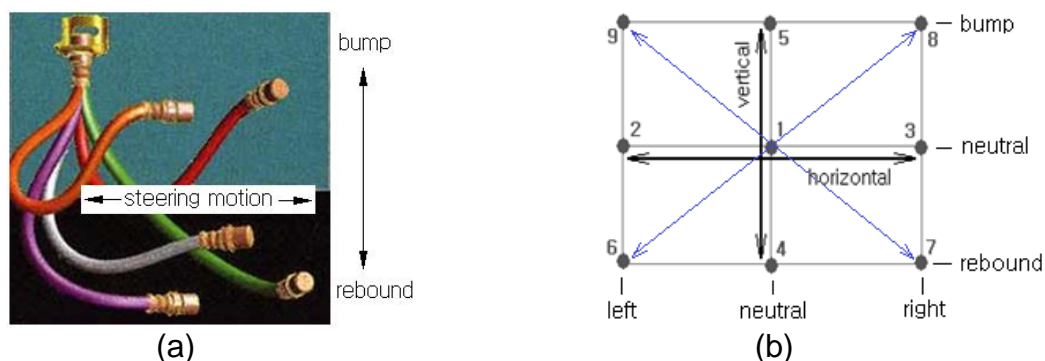


Fig.1 (a) Steering and bump/rebound motions of braking hose, (b) nine extreme positions of defining the cyclic paths

For a given braking hose, its deformation is not unique but diverse in aspects of the deformed configuration and the deformation magnitude, depending on the moving path of hose movable end. The hose deformation is not only large and complicated but also repetitive, so that the deformed braking hose may contact with other adjacent automotive parts and the hose durability deteriorates in proportional to the repetition number of cyclic deformations. The path of hose movable end is not easy to identify because it is diversely determined according to a combination of the tire steering motion and the bump/rebound motion of vehicle. In fact, its realistic and exact identification would be possible only by either the motion measurement using the vision system or 3-D multibody dynamics (MBD) simulation. However, even if possible, such measurement or MBD simulation requires the painstaking job for processing the numerous motion data.

For this reason, the path is rather simply defined using nine extreme positions shown in Fig. 1(b) that are determined by the tensor product of three positions in the steering mode and three positions in the bump/rebound mode. The neutral position corresponds to the straight driving without bump and rebound, and the left and right positions indicate the maximum steering in the left and right directions. Meanwhile, the bump and rebound indicate the maximum compression and stretching of tire in the vertical direction with respect to the vehicle. Two most representatives are the horizontal path 2-1-3 and the vertical 4-1-5, where the former corresponds to the left-neutral-right handling in cruising while the latter to the center acceleration and braking, respectively.

2. FIVE-LAYERED FABRIC BRAIDED RUBBER HOSE

Fig. 2(a) shows a five-layered reinforced braking hose composed of three rubber layers and two fabric braided layers. The unfold configuration of braided layer is represented in Fig. 2(b), where warp and fill tows are woven with the specific helix angle α_H . Each warp and fill tow are composed of three polyester cords, and the interfaces between warp and fill tows are also assumed to be perfectly bonded. The total number of warp and fill tows within a pitch p is defined by C_r and the diameter of base cord is denoted by $denia$ which is defined by the total weight in gram per 9,000m of cord. These material parameters as well as the helix angle are key parameters influencing the anisotropic behavior of braided layer.

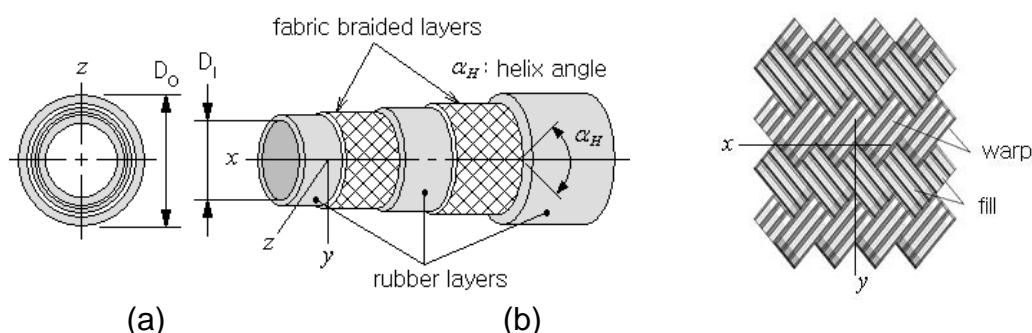


Fig. 2 Fabric braided rubber hose: (a) layer composition, (b) unfolded fabric braid

With the setting of material co-ordinates shown in Fig. 2(a), two fabric braided layers are modeled as an orthotropic material with the constitutive relation (Daniel and Ishai, 1994) given by

$$\begin{Bmatrix} \sigma_1 \\ \sigma_2 \\ \sigma_3 \\ \tau_{23} \\ \tau_{31} \\ \tau_{12} \end{Bmatrix} = \begin{bmatrix} D_{11} & D_{12} & D_{13} & 0 & 0 & 0 \\ D_{21} & D_{22} & D_{23} & 0 & 0 & 0 \\ D_{31} & D_{32} & D_{33} & 0 & 0 & 0 \\ 0 & 0 & 0 & D_{44} & 0 & 0 \\ 0 & 0 & 0 & 0 & D_{55} & 0 \\ 0 & 0 & 0 & 0 & 0 & D_{66} \end{bmatrix} \begin{Bmatrix} \varepsilon_1 \\ \varepsilon_2 \\ \varepsilon_3 \\ \gamma_{23} \\ \gamma_{31} \\ \gamma_{12} \end{Bmatrix} \quad (1)$$

with six diagonal terms defined by $D_{ii} = (1 - \nu_{jk}\nu_{kj})/E_j E_k \Delta$ and $D_{i+3i+3} = G_{ij}$. The other six off-diagonal terms are defined by

$$D_{ij} = \frac{\nu_{ji} + \nu_{ki}\nu_{jk}}{E_j E_k} \quad (i \rightarrow j \rightarrow k), \quad D_{kj} = \frac{\nu_{jk} + \nu_{ik}\nu_{ji}}{E_i E_j} \quad (k \rightarrow j \rightarrow i) \quad (2)$$

with $\Delta = (1 - \nu_{12}\nu_{21} - \nu_{23}\nu_{32} - \nu_{31}\nu_{13} - 2\nu_{12}\nu_{23}\nu_{31})/E_1 E_2 E_3$. Where, subscripts 1, 2 and 3 stand for x, y and z , respectively.

Meanwhile, the incompressible hyperelastic behavior of three rubber layers is modeled by a four-term Mooney-Rivlin material model which is expressed by the strain energy density functional $W(I_1, I_2, I_3)$ defined by

$$W(I_1, I_2, I_3) = C_{10}(I_1 - 3) + C_{01}(I_2 - 3) + C_{20}(I_1 - 3)(I_2 - 3) + \frac{\kappa}{2}(I_3 - 1)^2 \quad (3)$$

In which, I_i are the invariants of Green-Lagrange strain tensor and C_{ij} are the material dependent Mooney-Rivlin constants. The incompressibility of rubber is enforced by the last term on the right hand side of Eq. (3). The Mooney-Rivlin constants which were determined by the uniaxial tension test of rubber specimen may be referred to our previous paper (Cho et al., 2013).

3. FATIGUE EVALUATION

The cyclic motion of braking hose along a specific path produces the complex cyclic variations of strains and stresses, with the presence of mean strain and stress that are resulted from the pre-deformation caused when the braking hose is assembled at the neutral position. When the applied stresses generate predominantly elastic strain amplitudes, the mean stress effect can be taken into consideration by Basquin's mean stress correction method (Basquin, 1910; Karolczuk et al., 2013) given by $\sigma_{ar} = \sigma'_f (2N_f)^b$, where N_f is the fatigue life, σ'_f the fatigue strength coefficient, and b the fatigue strength exponent, respectively. Here, $\sigma_{ar} (= \sqrt{\sigma_{max}\sigma_a})$ denotes the equivalent

fully reversed stress amplitude defined in terms of the maximum stress σ_{max} and the stress amplitude σ_a . But, when the cyclic response of the material is within the elastic-plastic stress-strain range, the mean stress effect on fatigue life is based on the strain-life approach represented by

$$\frac{\Delta\varepsilon}{2} = \varepsilon_a = \frac{\Delta\varepsilon^e}{2} + \frac{\Delta\varepsilon^p}{2} = \frac{\sigma'_f}{E} (2N_f)^b + \varepsilon'_f (2N_f)^c \quad (4)$$

where ε_a is the strain amplitude, ε'_f the fatigue ductility coefficient, and c the fatigue ductility exponent. The modification of Eq. (4) which is used to predict the fatigue life for zero mean stress was made by several investigators (Smith et al., 1970; Ince and Glinka, 2011). The current study utilizes the Morrow model given by

$$\frac{\Delta\varepsilon}{2} = \frac{\sigma'_f - \sigma_m}{E} (2N_f)^b + \varepsilon'_f (2N_f)^c \quad (5)$$

By the way, this correction model is needed to be slightly modified for the current study because the large deformation analysis of braking hose is carried out using the Moonley-Rivlin hyperelastic material model by neglecting the plastic strain. Furthermore, the term σ'_f / E is replaced with a material-dependent fatigue parameter K_f which can be determined from the $\varepsilon - N$ curves shown in Fig. 3(a) in the log-log scale. Then, we have the modified Morrow model given by

$$\frac{\Delta\varepsilon}{2} = (K_f - \varepsilon_m) (2N_f)^b \quad (6)$$

Since strains and stresses at each material point exhibit the complex time histories composed of a number of harmonic cycles, as illustrated in Fig. 5(b), we employ the Palmgren-Minor cumulative damage law given by

$$D = \sum_{i=1}^{N_s} D_i, \quad D_i = \frac{n_i}{(N_f)_i} \quad (7)$$

to calculate the total accumulated fatigue damage D during a single deformation cycle along the specific cyclic path. Here, N_s is the total number of distinct harmonic strain cycles, D_i the accumulated fatigue damage by the i -th harmonic strain cycle, and n_i and $(N_f)_i$ the repetition number and the fatigue life of the i -th strain cycle, respectively. Then, the fatigue life N_f (cycles) at each material point within the braking hose along the specific path is calculated by $N_f = 1/D$. The fatigue life calculation is performed node by node using the signed nodal von Mises strains $\pm \varepsilon_{vm}$. The repetition numbers n_i of each distinct strain cycle are counted by the rainflow cycle counting method.

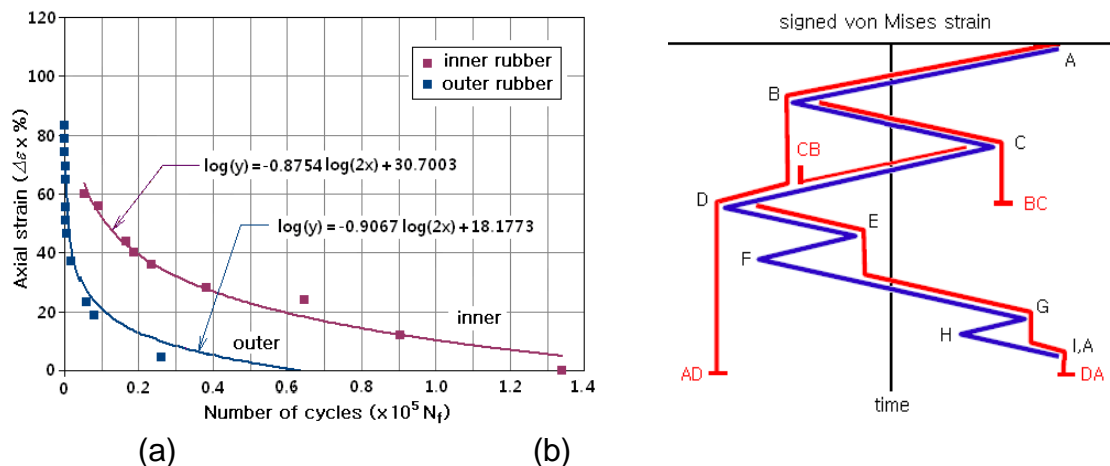


Fig. 3 (a) The $\varepsilon - N$ curves of two rubber layers, (b) rainflow cycle counting

4. NUMERICAL EXPERIMENTS

A five-layered braking hose of the length L of 230mm and the outer diameter D_o of 10.5mm is taken for the numerical experiments. The top end is clamped while the bottom end is forced to move along the predefined, where the center co-ordinates and rotations of the cross-section of the bottom end at nine extreme positions are referred to our previous paper (Cho et al., 2015) Referring to the previous Fig. 2(a), the thicknesses of five layers are as follows: $1.25, 0.30$ and 1.10mm for the outer, middle and inner rubber layers and 0.45mm for the outer and inner fabric braided layers. Two fabric braided layers are manufactured with PVA (poly vinyl alcohol) and the helix angles α_H , pitch p and C_r are as follows: $18.5\text{mm}, 24$ and 53.64° for the outer layer and $14.0\text{mm}, 20$ and 55.57° for the inner layer. The homogenized orthotropic material properties of the inner and outer fabric braided layers are given in our previous paper (Cho et al., 2013).

Three rubber layers are manufactured with EPDM (ethylene-propylene-diene-monomer), and the fatigue life is evaluated for the outer and inner rubber layers because both layers are weak to fatigue damage and play an important role in preventing the oil leakage. The entire braking hose is uniformly discretized with the total of 33,002 8-node hexahedron elements. Basically, the updated Lagrangian formulation is used to compute the increments of strain and stress during the hose large deformation along the cyclic paths, and the invariants of Green-Lagrange strain tensor in Mooney-Rivlin models were evaluated in the sense of total Lagrangian. Two fatigue parameters K_f and b in the modified Morrow model in Eq. (6) are found to be: 30.7003 and -0.8754 for the inner rubber layer and 18.1773 and -0.9067 for the outer rubber layer, respectively.

Fig. 4(a) represents the in-plane and out-of-plane deformed configurations of the braking hose for path 1 when the maximum in-plane deformation reaches the peak value. Those of the remaining three cyclic paths are given in Table 1. It is clearly observed that the maximum values δ_i and δ_o are quite different for different paths. Paths 1 and 3 produce relatively larger in-plane deformations, but conversely, the out-

of-plane deformations at both paths are shown to be insignificant. In case of the out-of-plane deformation, it is shown to be remarkable at paths 2 and 4. The maximum in-plane and out-of-plane deformations are largest at path 1 and 2, respectively, such that δ_I is 71.59mm while δ_O is 17.75mm.

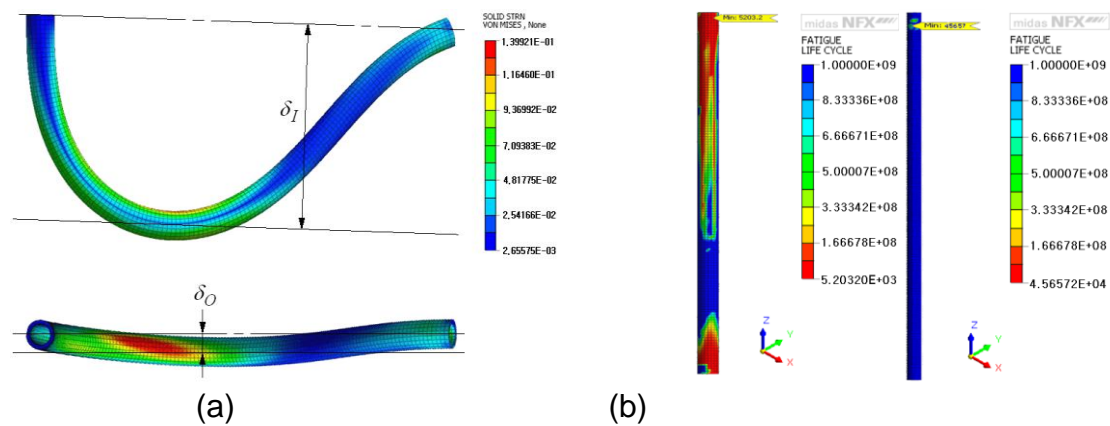


Fig. 4 Numerical results of path 1: (a) maximum in- and out-of-plane plane deformations, (b) fatigue life profiles

Table 1 Comparison of the hose deformations, the peak equivalent strains and stresses, and the critical fatigue lives to the cyclic path

Items		Cyclic paths			
		1	2	3	4
Maximum deformation (mm)	In-plane	71.59	41.66	70.01	59.52
	Out-of-plane	6.67	17.75	0.95	9.43
Peak equivalent strain		0.582	0.287	0.466	0.144
Peak effective stress (MPa)		4.992	2.485	5.664	1.142
Critical fatigue life (Cycles)	Outer rubber	4,806	21,623	5,735	12,412
	Inner rubber	45,657	133,765	54,482	168,151

Fig. 4(b) represents the fatigue life profiles of the outer and inner rubber layers for path 1. It is observed that the fatigue life of inner rubber layer is much higher than that of the outer rubber layer. This is also observed from Table 1 for the remaining three cyclic paths, which is because the magnitude of bending and torsional strain and stress decreases in inverse proportional to the radius of rubber hose. Meanwhile, it is found that both the peak equivalent strain and stress are remarkable at paths 1 and 3, which is because both paths produce relatively larger deformations. For all the paths, we observed the significantly high strain and stress in the upper one-third region and in the vicinity of lower movable end. The peak equivalent strain 0.582 was occurred in the vicinity of the upper fixed end at path 1, while the peak effective stress 5.664MPa appeared at the same point but at path 3. We observed that all the cyclic paths show the remarkably lower fatigue lives in the vicinity of upper fixed and lower movable ends because the equivalent strain is relatively larger in these regions. Regarding the hose path, it is found that the critical fatigue life is significantly lower at paths 1 and 3 when

compared with paths 2 and 4. As given in Table 1, path 1 shows the lowest critical fatigue life equal to 4,806 in the vicinity of upper fixed end.

CONCLUSION

In this paper, the large deformation and fatigue life of fabric braided composite rubber hose are investigated to the four representative cyclic paths. It has been observed that the maximum in-plane and out-of plane deformations and the critical fatigue lives are remarkably different for different cyclic paths. These parametric results would be usefully used for the layout and durability design of braking hose.

ACKNOWLEDGEMENT

This research was supported by Basic Science Research Program through the National Research Foundation of Korea (NRF) funded by the Ministry of Education (Grant No. NRF-2014R1A1A2055820).

REFERENCES

- Basquin, O.H. (1910), "The exponential law of endurance tests", *Proc. Am. Soc. Test. Mater.*, **10**, 625-630.
- Cho, J.R., Song, J.I. and Choi, J.H. (2006), "Prediction of effective mechanical properties of reinforced braid by 3-D finite element analysis", *Key Eng. Mater.*, **306-308**, 799-804.
- Cho, J.R., Jee, Y.B., Kim, W.J., Han, S.R. and Lee, S.B. (2013), "Homogenization of Braided Fabric Composite for Reliable Large Deformation Analysis of Reinforced Rubber Hose," *Composites: Part B*, **53**, 112-120.
- Cho, J.R., Yoon, Y.H., Seo, C.W., Kim, Y.G. (2015), "Fatigue life assessment of fabric braided composite rubber hose in complicated large deformation cyclic motion," *Finite Elem. Anal. Des.*, **100**, 65-76.
- Chuda-Kowalska, M. and Garstecki, A. (2016), "Experimental study of anisotropic behavior of PU foam in sandwich panels", *Steel Comp. Struct.*, **20**(1), 43-56.
- Daniel, I.M. and Ishai, O. (1994), *Engineering Mechanics of Composite Materials*, Oxford University Press, New York.
- Entwistle, K.M. (1981), "The behavior of braided hydraulic hose reinforced with steel wires", *Int. J. Mech. Sci.*, **23**, 229-241.
- Ince, A. and Glinka, G. (2011), "A modification of Morrow and Smith-Watson-Topper mean stress correction models", *Fatigue Fract. Eng. Mater. Struct.*, **34**(11), 854-867.
- Karolczuk, A., Kowalski, M., Bariski, R. and Zok, F. (2013), "Fatigue phenomenon in explosively welded steel-titanium clad components subjected to push-pull loading", *Int. J. Fatigue*, **48**, 101-108.
- Smith, K.N., Watson, P., Topper, T.H., "A stress-strain function for the fatigue of materials," *J. Mater.*, **5**, 767-778, 1970.
- Xu, L., Kim, S.J. Ong, C.H. and Ha, S.K. (2012), "Prediction of material properties of biaxial and triaxial braided textile composites", *J. Composite Mater.*, **46**(18), 2255-2270.